Mixed Valence Systems

$$A \sim B + h\nu \rightarrow A^{+} \sim B^{-}$$

$$A \sim B + h\nu \rightarrow A^{*} \sim B \rightarrow A^{+} \sim B^{-}$$

$$K_c = \exp\frac{RT\Delta E}{nF} = \exp\frac{\Delta E}{25.69} \quad \text{at } 298\,\text{K}$$

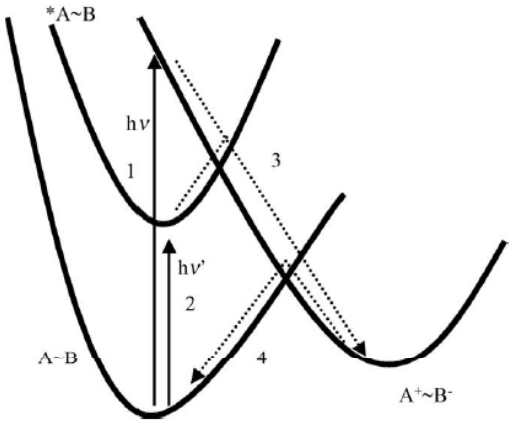

Fig. 4. Relationship between optical (1), photo-induced (2 and 3), and thermal back (4) electron transfer processes in supramolecular species.

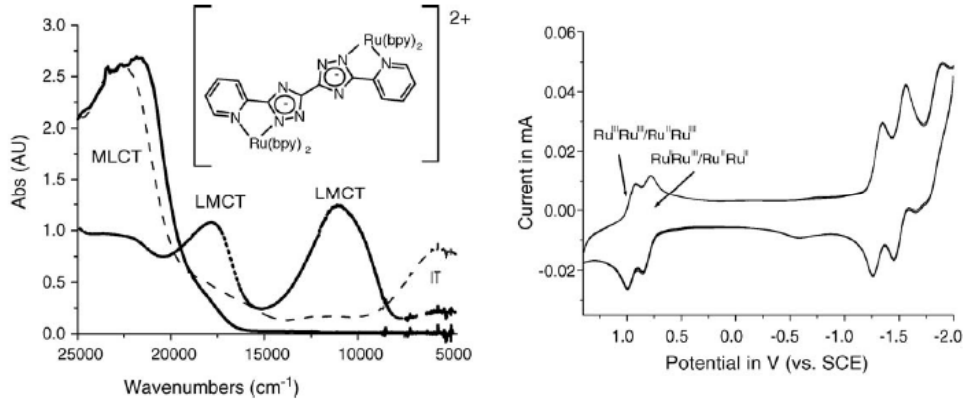

Fig. 3. Left: visible and near-IR absorption spectra of a binuclear ruthenium complex in acetonitrile (0.1 M TEAP) at 0.60 V (solid line), 1.00 V (d 1.10 V (dotted line) vs. SCE. Right: cyclic voltammetry at 0.1 V s^{-1}. Reprinted with permission from [6d]. Copyright [2002] American Chemical S

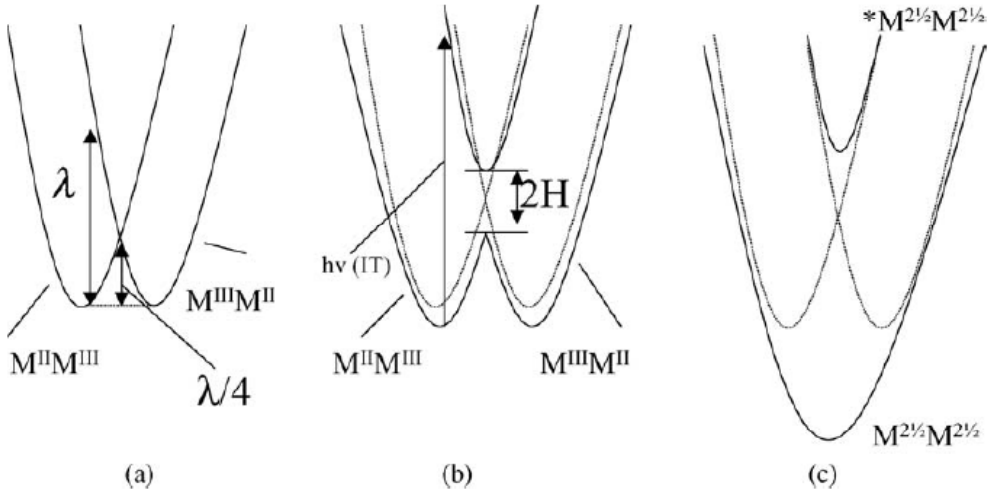

Fig. 5. Potential energy curves for a symmetric mixed valence compound showing: (a) negligible, (b) weak, and (c) strong electronic coupling. In the case of (b) and (c) the dashed lines represent the zero order states [76].

Basic Analytical Electrochemistry

- The fundamental process in electrochemistry is the transfer of electrons between the electrode surface and molecules in the solution adjacent to the electrode surface (*heterogeneous electron transfer*)

- One quantity that is particularly important in electrochemical experiments is *current* (**i**), and the current/per unit area is referred to as (**amps/cm^2**). Current density is the more fundamental quantity, since it is independent of the electrode surface area.

- Since current results from a chemical substance dissolved in the solution adjacent to the electrode surface the probability of a molecule or ion reacting at the electrode surface is directly related to the concentration. Therefore, current density is directly proportional to the concentration.

- The differential form of Faraday's Law [$\mathbf{i_F = nF(}d\mathbf{N/}d\mathbf{t)}$] shows that the rate at which electrons are moved across the electrode-solution interface (i.e., the current) is directly related to the rate of the reaction occurring at that interface. Therefore, when we measure the Faradaic current, we are also measuring the rate of a chemical reaction. It should be noted that there are multiple steps involved in an electrochemical reaction, such as the electron transfer reaction, transport of molecules from the bulk solution to the electrode surface, and chemical reactions coupled to the electron transfer reaction.

- The total current observed at the electrode surface is a summation of currents, including the Faradaic currents for the analyte, the electrolyte, and the electrode material, as well as the capacitive current. All but the first of these currents are generally undesirable, and attention must be given to minimizing their effects.

- If we integrate a rate, we obtain an amount. From the integrated form of Faraday's Law [$\mathbf{(Int)i_F}\, d\mathbf{t = nFN = Q}$] we can see the total amount of electricity passed (**Q** - the charge, measured in units of Coulombs) is proportional to the number of moles **N** of material processed by the electrochemical reaction.

- The fundamental reaction in electrochemistry is the equilibrium between two species (O and R) that are interconverted by the transfer of an electron:

$$O + e^- \rightleftharpoons R$$

- The position of the equilibrium is determined by the concentration of O and R which can be controlled by an external force, i.e. applied potential. The applied potential is thus a thermodynamic driving force.
- There is a unique situation in which the concentration of O and R are equal. This occurs at the formal reduction potential $E^{o'}$. This value provides a convenient index of the relative strength of an oxidant/reductant.
- The half-wave potential ($E_{½}$) can be readily obtained from the midpoint between the two peak potentials for a reversible (*or quasi-reversible*) redox couple. This value is characteristic of a redox couple and is typically within a few mV of the formal potential $E^{o'}$ for the couple according to the **Nernst** equation (the ratio of the diffusion coefficients D_{ox} and D_{Red} is usually very close to unity).

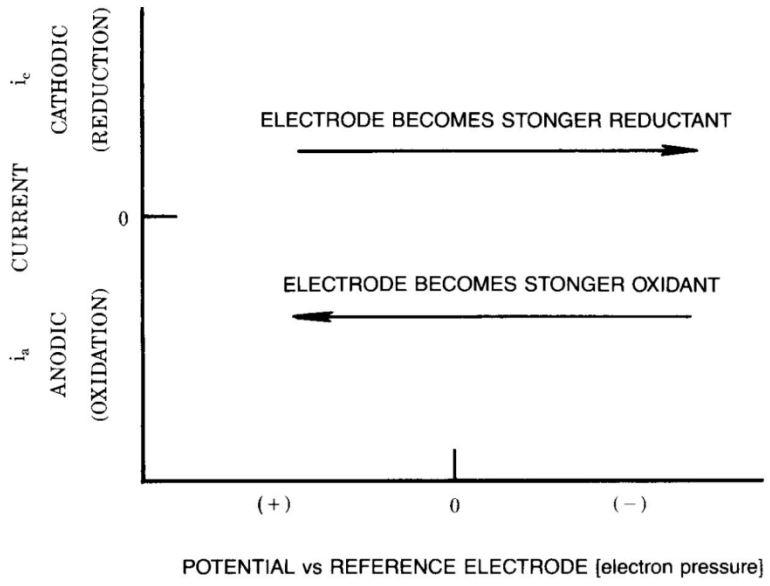

$$E_{1/2} = E^{o'} - \frac{RT}{2nF} \ln \frac{D_{Ox}}{D_{Red}}$$

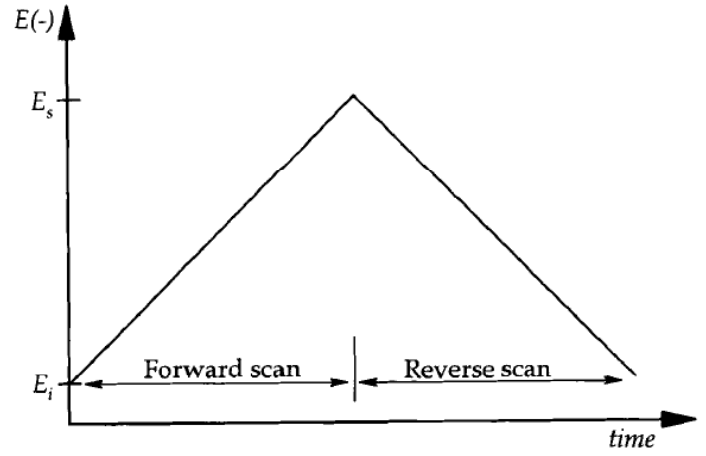

A typical potential excitation waveform used in CV.

4196 *Organometallics* **2009,** *28,* 4196–4209
DOI: 10.1021/om9002945

ORGANOMETALLICS
Article

Charge Delocalization in a Heterobimetallic Ferrocene−(Vinyl)Ru(CO)-Cl(P^iPr_3)$_2$ System†

Konrad Kowalski,*[,‡,§] Michael Linseis,[§] Rainer F. Winter,*[,§] Manfred Zabel,[§] Stanislav Záliš,*[,⊥] Harald Kelm,[△] Hans-Jörg Krüger,[△] Biprajit Sarkar,[▽] and Wolfgang Kaim[▽]

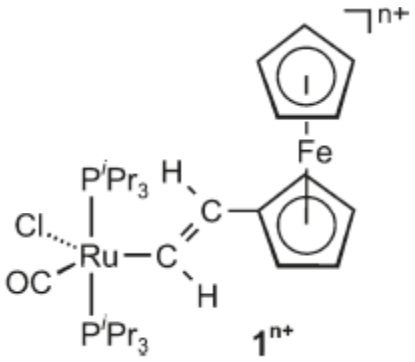

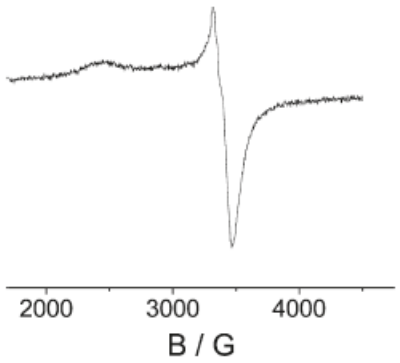

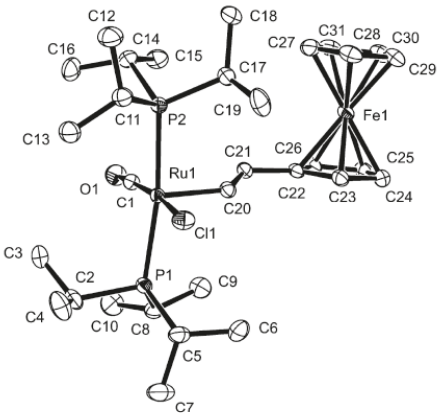

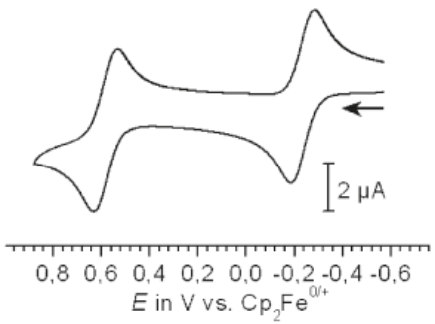

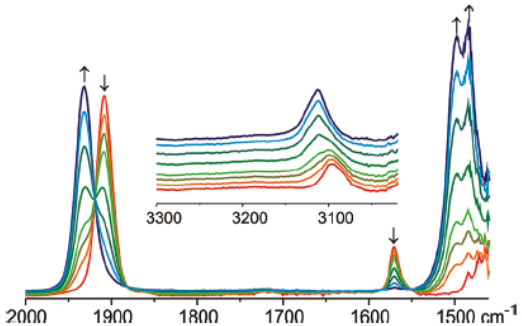

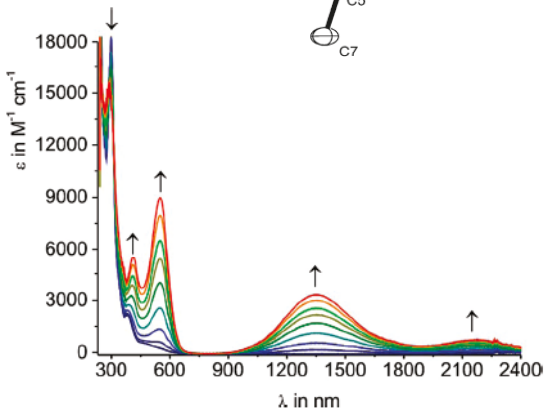

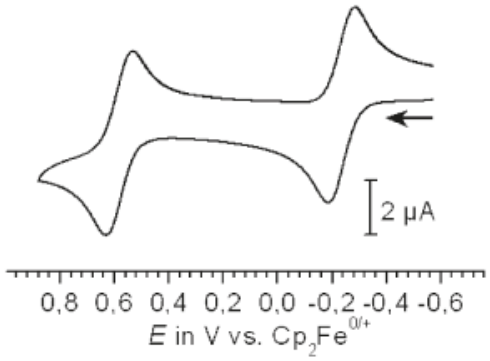

Figure 2. Voltammogram of **1** (NBu_4PF_6, 0.1 M, CH_2Cl_2, rt) at $v = 0.1$ V/s.

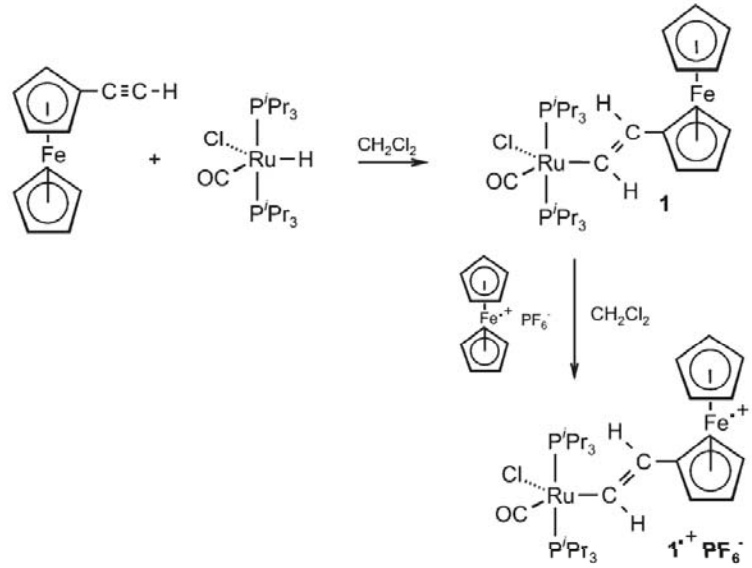

Complex **1** undergoes two consecutive one-electron oxidations at half-wave potentials of -0.235 and 0.580 V as measured against the internal ferrocene/ferrocenium redox standard (Figure 2). Both waves show all attributes of uncomplicated Nernstian-type redox couples such as identical peak-to-peak separations, half-widths, and peak current functions as the internal ferrocene standard. The apparent stability of **1** in three oxidation states and the presence of charge-sensitive spectroscopic labels on the ruthenium (ν(CO)) and ferrocene (ν(CH, Cp)) sites prompted us to study the spectroscopic changes accompanying stepwise oxidation.

The low first oxidation potential of -235 mV against the Fc/Fc^+ couple and the good stability of $1^{\bullet+}$ on even the extended time scale of bulk electrolysis suggested that this radical cation constitutes a viable synthetic target. Thus, $1^{\bullet+}PF6^-$ was obtained in nearly quantitative yield as a violet, air-stable powder when a solution of 1 in CH_2Cl_2 was treated with Fc^+PF6^- at room temperature (Scheme 1). As expected, the ^1H NMR spectrum of paramagnetic $1^{\bullet+}PF6^-$ shows only broad signals (see Experimental Section). Solution IR, UV/vis/NIR, and ESR spectra of pure $1^{\bullet+}PF6^-$ are identical to those obtained for electrogenerated $1^{\bullet+}$.

Optically transparent thin layer electrolysis (OTTLE) and UV-vis spectroelectrochemical cells

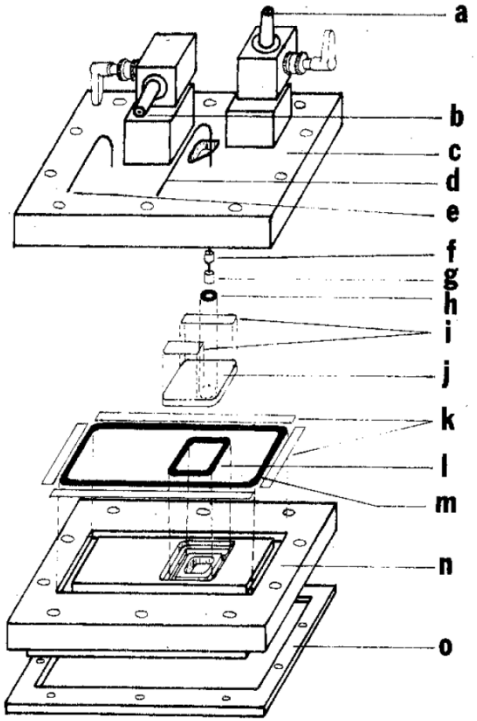

Figure 1. Thin-layer spectroelectochemical cell with demountable planar OTE: (a) solution inlet valve; (b) reference electrode valve; (c) upper Lucite plate; (d) copper wire for OTE contact; (e) silver wire auxiliary electrode; (f) rubber compression sleeve; (g) brass OTE contact; (h) O-ring; (i) Teflon tape; (j) OTE; (k) Teflon tape; (l) OTE O-ring; (m) perimeter O-ring; (n) lower Lucite plate; (o) aluminum retainer. The quartz window, which is located on the underside of the upper plate opposite of OTE, is not shown.

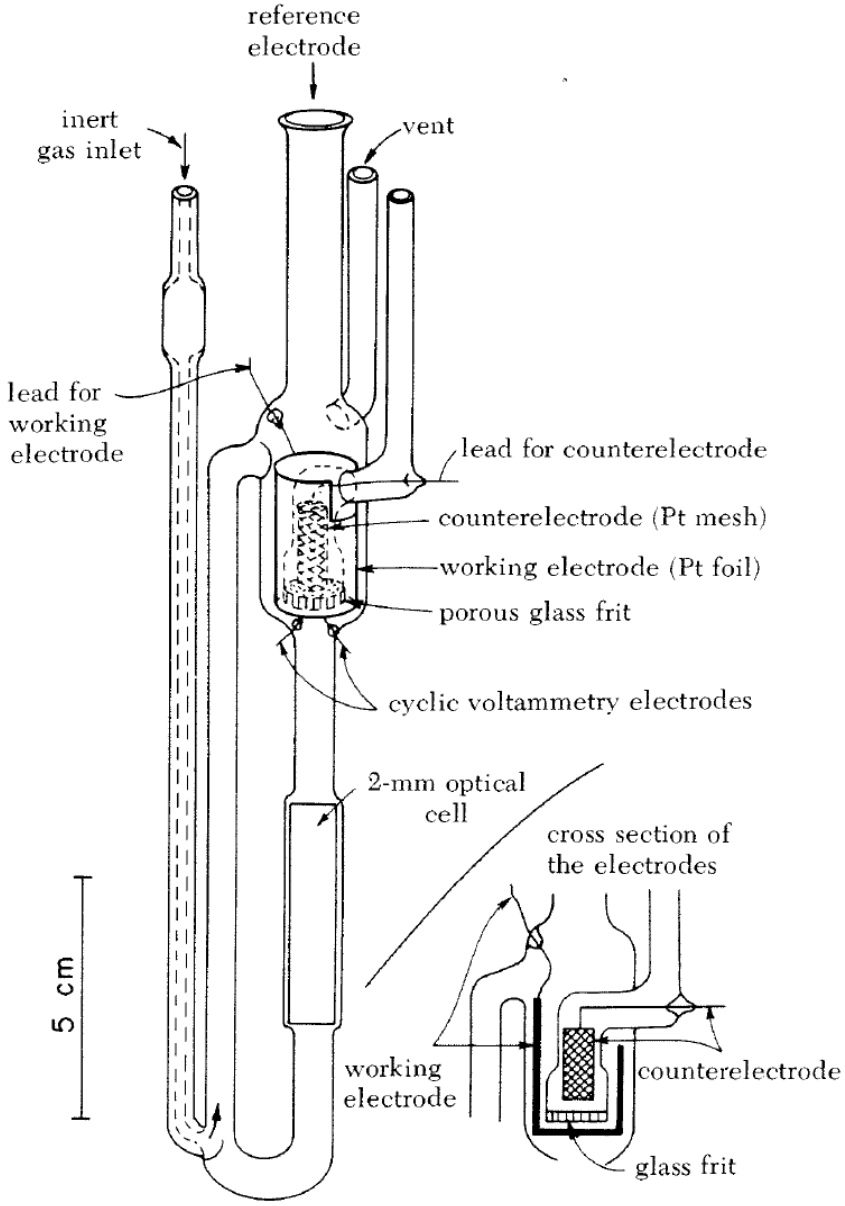

Figure 1. Electrooptical cell for controlled potential electrolysis, cyclic voltammetry, and optical measurements.

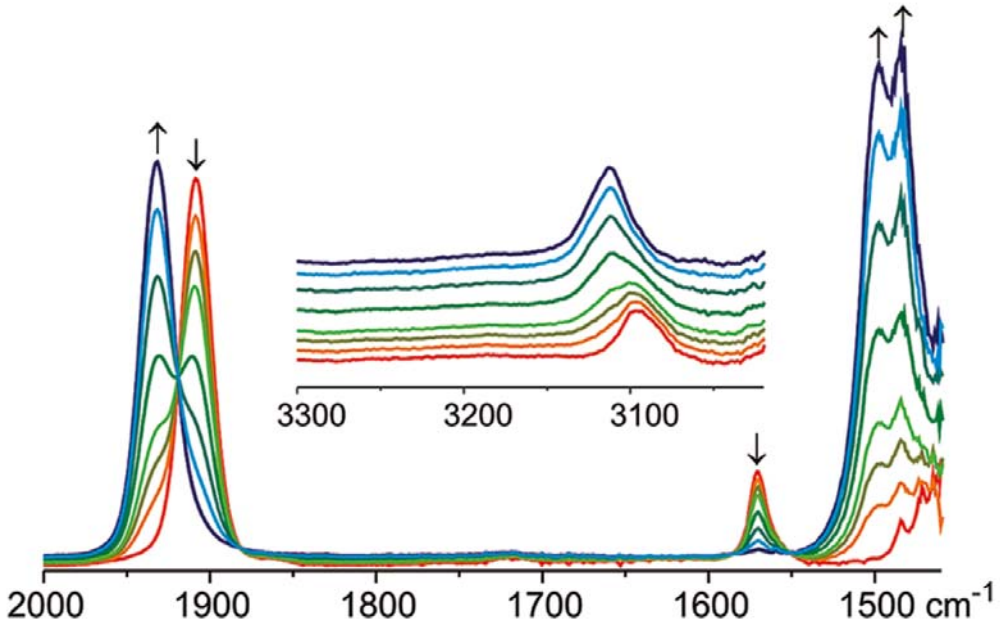

Figure 3. IR spectroscopic changes in the mid-IR upon the first oxidation of complex **1** (1,2-$C_2H_4Cl_2$/NBu_4PF_6) at r.t.

The most characteristic changes in the IR spectra upon the first oxidation are the ν(CO) shift of the ruthenium-bonded carbonyl ligand from 1908 to 1932 cm^{-1} and the replacement of the medium intense 1571 cm^{-1} absorption of the vinyl substituent by much stronger absorptions at 1498 and 1485 cm^{-1} (Figure 3 and Table 2). Also of note is the shift of the cyclopentadienyl CH stretch from 3096 to 3110 cm^{-1} (see inset of Figure 3). There are clear isosbestic points, and neutral 1 was obtained in quantitative spectroscopic yield when the solution was reduced back after the first oxidation had gone to completion.

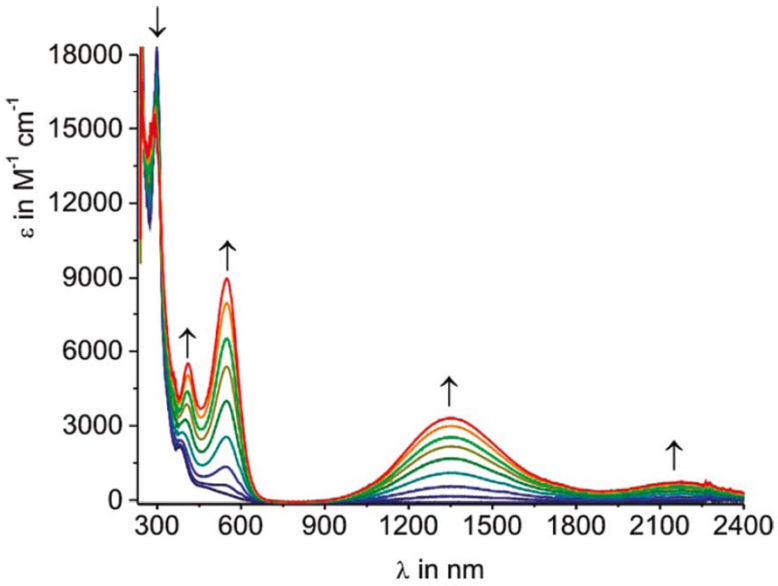

Figure 5. Spectroscopic changes during the first oxidation of **1** (1,2-$C_2H_4Cl_2$, NBu_4PF_6, rt).

- The electronic spectrum of neutral **1** is rather unremarkable, featuring an intense π→π* band at 300 nm and a weaker absorption at 381 nm, which are associated with the ferrocene and the (vinyl)ruthenium chromophore. Two overlappingbands at lower energy are associated with Fe→(vinyl)ruthenium charge-transfer and a d/d-type transition within the ferrocene nucleus.
- One-electron oxidation to $1^{\bullet+}$ in the 1,2-$C_2H_4Cl_2$/NBu_4PF_6 electrolyte caused the growth of new absorptions at 281, 413, 550, 1349, and 2164 nm(Figure 5), the latter two of which correspond to the NIR bands that were also observed in our IR measurements.

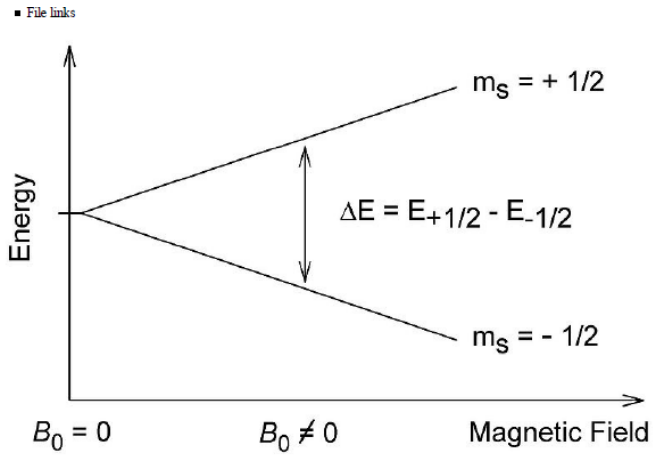

$$h\nu = g_e \mu_B B_0$$

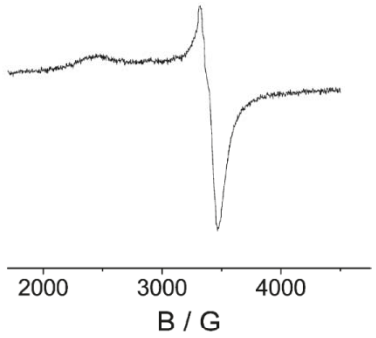

Figure 7. ESR spectrum of electrogenerated $\mathbf{1}^{\bullet+}$ in CH_2Cl_2/NBu_4PF_6 at T = 110 K.

In real systems, electrons are normally not solitary, but are associated with one or more atoms.
There are several important consequences of this:

- An unpaired electron can gain or lose angular momentum, which can change the value of its *g*-factor, causing it to differ from g_e. This is especially significant for chemical systems with transition-metal ions.
- If an atom with which an unpaired electron is associated has a non-zero nuclear spin, then its magnetic moment will affect the electron. This leads to the phenomenon of hyperfine coupling, analogous to J-coupling in NMR, splitting the EPR resonance signal into doublets, triplets and so forth.
- Interactions of an unpaired electron with its environment influence the shape of an EPR spectral line. Line shapes can yield information about, for example, rates of chemical reactions.
- The *g*-factor and hyperfine coupling in an atom or molecule may not be the same for all orientations of an unpaired electron in an external magnetic field. This anisotropy depends upon the electronic structure of the atom or molecule (e.g., free radical) in question, and so can provide information about the atomic or molecular orbital containing the unpaired electron.

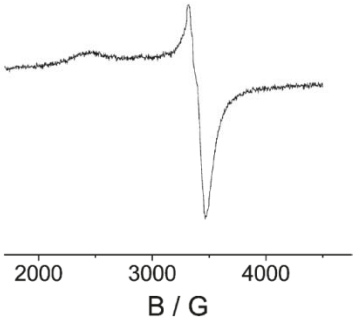

Figure 7. ESR spectrum of electrogenerated $\mathbf{1}^{\bullet+}$ in CH_2Cl_2/NBu_4PF_6 at T = 110 K.

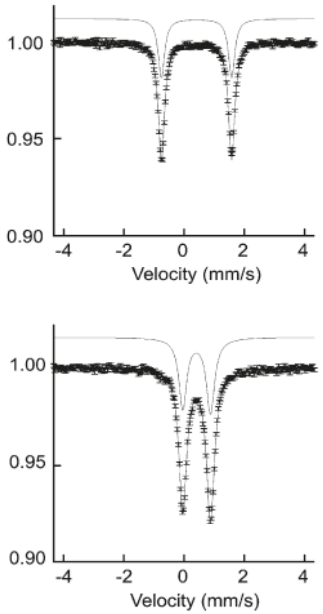

Figure 9. Moessbauer spectra of powdered solid **1** (top) and $\mathbf{1}^{\bullet+}\mathbf{PF_6^-}$ (bottom) at T = 25 K. Isomeric shifts are relative to the source with δ = −0.11 with respect to α-Fe.

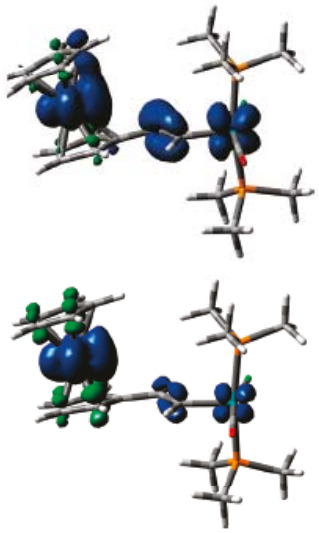

Figure 12. DFT-calculated spin densities for $\mathbf{1}^{\mathbf{Me}\,\bullet+}$ using the BPW91 (top) or PBE0 (bottom) functional.

ESR spectroscopy of $1^{\bullet+}$ that was electrogenerated in an ESR tube gave no signal at room temperature but an intense axial signal with $g_{\parallel}$=2.80 and $g_{\perp}$=1.984 when frozen in an CH_2Cl_2 matrix at 110 K (Figure 7).

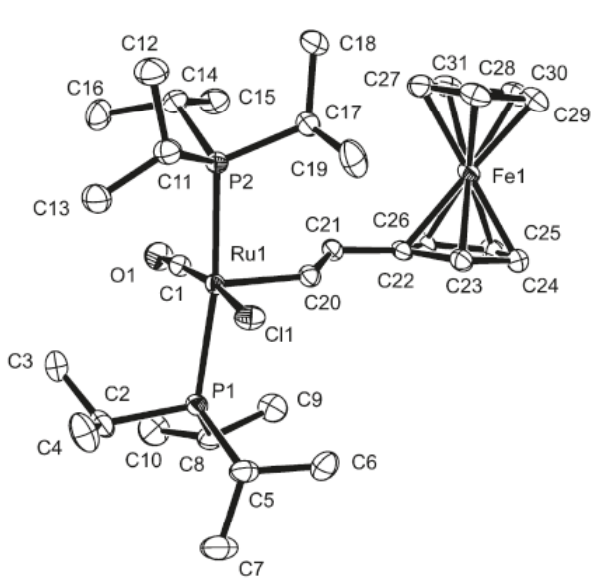

Figure 1. ORTEP view of complex **1** (solvent-free crystal). Hydrogen atoms are omitted for clarity. Ellipsoids are drawn at a 50% probability level. Selected bond lengths (Å) and angles (deg): Ru−C1, 1.820(2); Ru−Cl, 2.4380(5); Ru−C20, 1.996(2); Ru−P1, 2.4106(5); Ru−P2, 2.3947(5); C20−C21, 1.339(3); C21−C22, 1.463(3); P1−Ru−P2, 170.05(2); Cl−Ru−C1, 171.73(6); Ru−C1−O1, 178.3(2); Cl−Ru−C20, 98.38(5); Ru−C20−C21, 134.8(2); C20−C21−C22, 123.6(2).

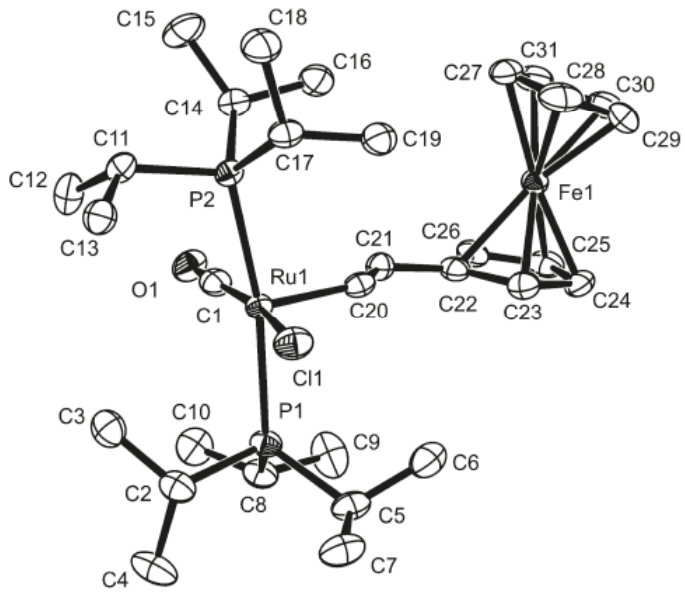

Figure 8. ORTEP view of $\mathbf{1}^{\bullet+}$ (solvent-free crystal). Hydrogen atoms are omitted for clarity. Ellipsoids are drawn at a 50% probability level. Selected bond lengths (Å) and angles (deg): Ru−C1, 1.851(4); Ru−Cl1, 2.4305(10); Ru−C20, 1.955(4); Ru−P1, 2.4260(10); Ru−P2, 2.4252(10); C20−C21, 1.354(5); C21−C22, 1.458(5); P1−Ru−P2, 167.86(4); Cl1−Ru−C1, 168.16(13); Ru−C1−O1, 176.2(4); Cl1−Ru−C20, 102.50(9); Ru−C20−C21, 134.2(3); C20−C21−C22, 124.8(3).

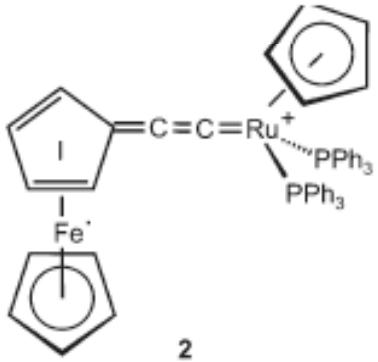

2

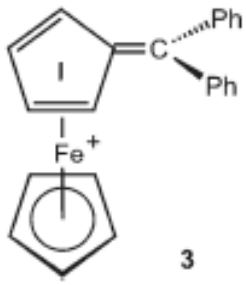

3

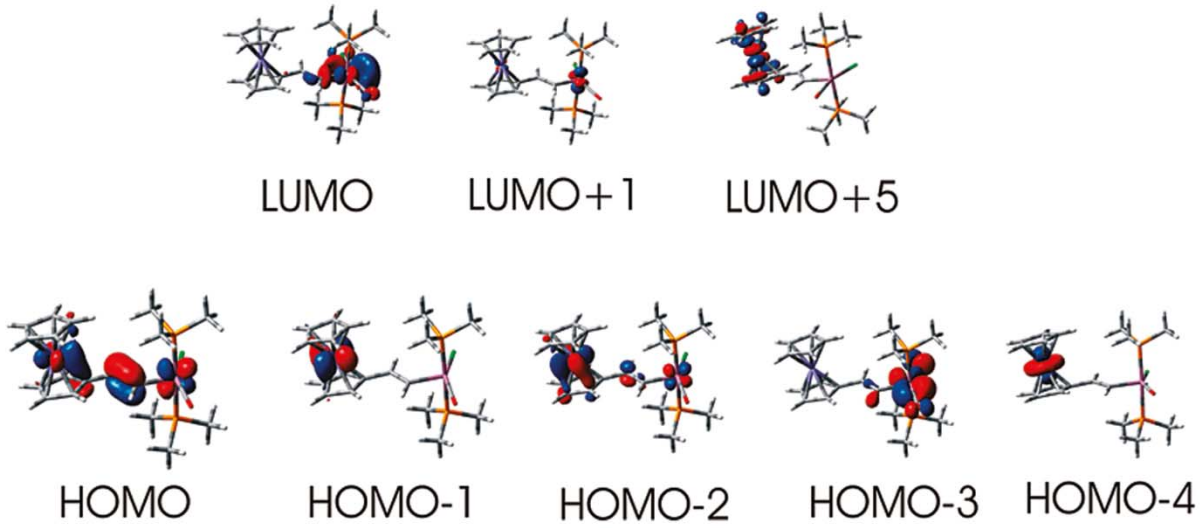

Figure 10. Frontier MOs involved in calculated excitations of $\mathbf{1}^{\mathbf{Me}}$.

- DFT calculations indicate that the HOMO of neutral **1** is delocalized across the entire metal-organic π-system.
- One-electron oxidation removes electron density from essentially the delocalized HOMO. DFT-calculated spin densities of **1Me**$^{\bullet+}$confirm spin delocalization across the entire Ru-CH=CH-Fc$^{\bullet+}$ system.

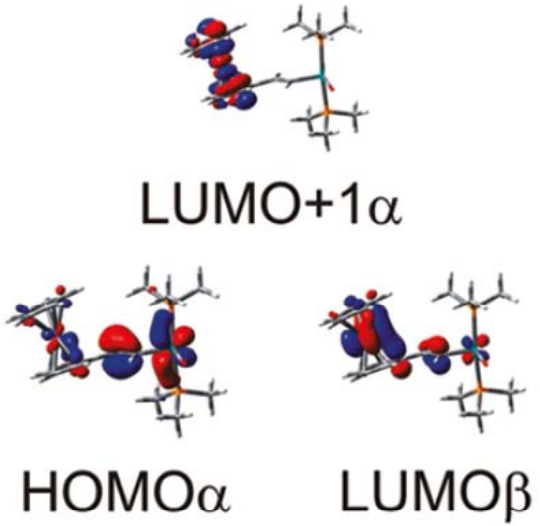

Chart 3. Resonance Structures of $1^{\bullet+}$

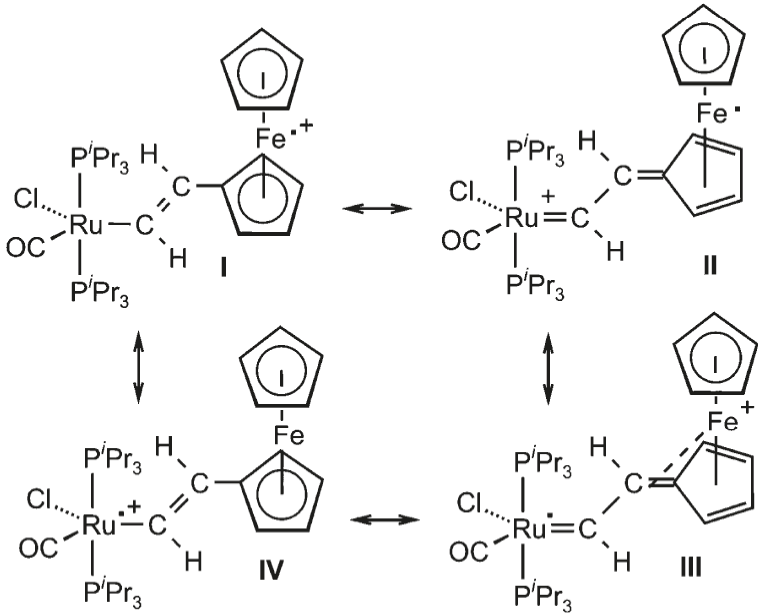

Chart 4